

# POEv2: a flexible and robust framework for generic line segment detection and wireframe line segment detection

Chenguang Liu, Chisheng Wang\*, Yuhua Cai, Chuanhua Zhu, and Qingquan Li

**Abstract**—Line segment detection in images has been studied for several decades. Existing line segment detectors can be roughly divided into two categories: generic line segment detectors and wireframe line segment detectors. Generic line segment detectors aim to detect all meaningful line segments in images and traditional approaches usually fall into this category. Recent deep learning based approaches are mostly wireframe line segment detectors. They detect only line segments that are geometrically meaningful and have large spatial support. Due to the difference in the aim of design, the performance of generic line segment detectors for the task of wireframe line segment detection won't be satisfactory, and vice versa. In this work, we propose a robust framework that can be used for both generic line segment detection and wireframe line segment detection. The proposed method is an improved version of the Pixel Orientation Estimation (POE) method. It is thus named as POEv2. POEv2 detects line segments from edge strength maps, and can be combined with any edge detector. We show in our experiments that by combining the proposed POEv2 with an efficient edge detector, it achieves state-of-the-art performance on three publicly available datasets.

**Index Terms**—Generic line segment detection, wireframe line segment detection, POEv2, deep learning, edge detector.

## I. INTRODUCTION

LINE segments are important features in images as many man-made objects such as buildings and roads can be described using line segments. A lot of vision tasks such as vanishing point estimation [1], 3D reconstruction [2], image segmentation [3], object detection [4], and stereo matching [5], can greatly benefit from an accurate detection of line segments in images. Due to the importance of line features in images, line segment detection has attracted the attention of many researchers and plenty of algorithms have been developed to detect line segments in images. Traditional approaches usually first compute an edge map or compute the gradient of each pixel, and then detect line segments in images using Hough transform [6], [7] or perceptual grouping [8], [9]. Even though the gradient computation methods used in these methods may

not be able to give a good separation between edge and non-edge pixels, their detections can be very accurate and the number of false detections can be controlled through the use of a strong validation criterion [9], [10], [11]. These methods are designed to detect all meaningful line segments in images and they can be excellent generic line segment detectors. However, sometimes it may be necessary to distinguish line segments that are important for understanding the shape of regular objects or geometric layout of the scene from other line segments [12]. Inferring only this kind of line segments is difficult for traditional approaches as they could be only a small subset of line segments in images. This kind of line segments are referred to as wireframe line segments [12], and a dataset, the ShanghaiTech dataset, have been created for training and evaluation of wireframe line segment detection algorithms [12]. Ever since the creation of the ShanghaiTech dataset, many methods have been developed to detect wireframe line segments based on deep learning. Some approaches combine the detection of wireframe line segments with the detection of junctions [13], [14]. Candidate wireframe line segments may be generated through the training of a convolutional neural network or by learning the connectivities among predicted junctions. Another line work adopts an attraction field representation of line segment maps and compute candidate line segments from the predicted attraction field maps [15], [16], [17], [18]. Some other approaches adopted either a tri-point representation of line segment [19], or represented a line segment using their center, length, and angle [20], and treated the detection of line segment similar to an object detection problem. These approaches achieve excellent performance in the ShanghaiTech dataset, while their generalization capability requires further study. Besides, many meaningful line segments may not be detected by these methods as they are not labeled in the ShanghaiTech dataset. For instance, line segments corresponding to sofa, chairs, and humans are not annotated in the ShanghaiTech dataset [12], while they are meaningful objects in images. This could be an important reason why none of recent deep learning based wireframe line segment detectors evaluates their performance on the generic line segment detection dataset, the YorkUrban-LineSegment dataset [11].

Indeed, detecting generic line segments and detecting wireframe line segments should be considered as different tasks. A generic line segment detector will produce many false detections for the task of wireframe line segment detection. On the contrary, many true line segments could be missing

\* represents the corresponding author.

Chenguang Liu (Email: chenguang.liu.light@outlook.com), Chisheng Wang (Email: wangchisheng@szu.edu.cn), Yuhua Cai, Chuanhua Zhu, and Qingquan Li are with the School of Architecture and Urban Planning, Shenzhen University, China. Chenguang Liu, Chisheng Wang, Chuanhua Zhu, and Qingquan Li are also with the Ministry of Natural Resources (MNR) Key Laboratory for Geo-Environmental Monitoring of Great Bay Area & Guangdong Key Laboratory of Urban Informatics, and the Guangdong Laboratory of Artificial Intelligence and Digital Economy (SZ), China.

when applying a wireframe line segment detector to the task of generic line segment detection. In this work, we propose a robust and flexible framework that can be used for both generic line segment detection and wireframe line segment detection. Specifically, line segments are closely related to edges. They are defined to be locally straight edges: generic line segments are straight parts of all meaningful edges while wireframe line segments are straight parts of wireframe edges. As it is quite easy to train a generic edge detector and a wireframe edge detector, only if we could design a robust method to extract line segments from edge predictions, the proposed method can be used for both generic line segment detection and wireframe line segment detection.

Pixel Orientation Estimation (POE) method [21] is a line segment detection framework that detects line segments from binary edge maps. It is developed based on two intuitions: first, an edge pixel should have the same orientation as the line segment passing through it; second, if we count the number of edge pixels along different orientations starting from an edge pixel, the orientation that gives the maximum number of counts should be aligned with direction of the line segment passing through it. The orientation of edge pixels can thus be estimated by counting the number of edge pixels along a set of orientations. With the estimated orientation of edge pixels, candidate line segments can be obtained through a region growing algorithm that groups edge pixels sharing the same orientation up to an angle tolerance. Finally, candidate line segments would be considered as true detections if their support regions have sufficient number of edge pixels. In this work, we show that POE achieves competitive performance for generic line segment detection and achieves state-of-the-art performance for wireframe line segment detection when combining it with an efficient edge detector. We then propose an improved version of POE, named as POEv2, and show that by combining it with the same edge detector, POEv2 sets new state-of-the-art for both generic line segment detection and wireframe line segment detection. Unlike POE which simply binarizes the edge strength maps using a threshold, POEv2 fully exploits the valuable information contained in edge strength maps (pixels with higher values are more likely to be true edge pixels). Besides, we propose a novel Guided Region Growing algorithm to improve the accuracy of region growing. The proposed Guided Region Growing algorithm dynamically updates the angle of potential line segments, and guides the direction in which the region growing algorithm should go using the updated angle. Comprehensive experiments show that POEv2 achieves higher accuracy than POE with the help of these elaborate designs.

The contributions of this work can be summarized as follows:

- We clarify the difference between generic line segment detection and wireframe line segment detection, as most recent deep learning based wireframe line segment detectors compare their performance with generic line segment detectors for the task of wireframe line segment detection without considering the distinction between them.
- We show that by combining POE with a trained edge detector, it achieves competitive performance for generic

line segment detection and state-of-the-art performance for the task of wireframe line segment detection.

- We propose an improved version of POE based on a novel Guided Region Growing algorithm, the proposed POEv2, which sets new state-of-the-art for both generic line segment detection and wireframe line segment detection.
- Similar to POE, the proposed POEv2 can be combined with any edge detector, which means that its performance can be improved further if a more powerful edge detector is used.

The rest of this paper is organized as follows: Section II introduces previous methods for generic line segment detection and wireframe line segment detection; Section III provides a detailed description of the proposed POEv2, and experiments on three datasets are provided in Section IV; finally, conclusions of this paper are given in Section V.

## II. RELATED WORK

Due to the importance of line segments in images, a significant number of studies have been published on the topic of line segment detection. Traditional approaches are mostly generic line segment detectors and they aim to detect all meaningful line segments in images. Recent deep learning methods are mostly wireframe line segment detectors and they focus on the detection of line segments describing scene structures. Here we give a brief review of methods on both topic.

### A. Generic line segment detectors

In the early stage, the classical way to detect line segments from images was based on the Hough transform [6], [7]. Hough transform was designed to detect line segments from binary edge maps or edge strength maps. Therefore, an edge detector such as [22] was usually first applied to process the input images, and then Hough transform was used to detect line segments. It searches for possible lines in a parameter space by counting the number of edge pixels contributing to each line. Line segments are then obtained by cutting lines with thresholds. Even though Hough transform works well in some cases, it suffers from several drawbacks. First, in complicated regions where dense edges are detected, Hough transform may generate many false positives [9], [11]. Second, multiple responses of a line segment may be detected by Hough transform due to the digitization effects of line segments in images [23], [21]. Third, the parameter values of Hough transform usually have to be manually tuned for each image, and it is difficult to find a set that works well globally [23]. Even though several approaches have been proposed to improve the drawbacks of Hough transform [24], [25], [26], their performance still has a large room for improvement. Later on, [8] proposed to detect line segments by grouping pixels having similar gradient orientations. On the basis of it, LSD [9] proposed a fast line segment detector by introducing a strong validation criterion based on the Helmholtz principle and the *a contrario* model [10]. Thanks to the strong validation criterion, LSD is able to strictly control the number of false detections and require little parameter tuning. Despite its efficiency, true line segments may be rejected by the strong validation criterion

in complex regions [11]. Linelet [11] proposed a linelet-based representation of line segments in images to exploit the intrinsic properties of line segments in images caused by digitization effect, where a linelet is defined as a set of either horizontally or vertically connected pixels. On the basis of the linelet-based representation, a probabilistic validation framework and an aggregation framework are proposed, contributing to the final line segment detection framework. Recently, DeepLSD [27] proposed to combine the merits of traditional approaches and deep learning methods for robust line segment detection. It computes a surrogate gradient magnitude and angle from a line attraction field generated by deep networks. Then the computed gradient magnitude and angle are fed into traditional hand-crafted methods to detect line segments.

### B. Wireframe line segment detectors

In [12], the authors created the ShanghaiTech dataset by labeling the line segments associated with scene structures. The line segments corresponding to shadows, irregular or curved objects such as sofa and humans are not labeled. Therefore, we call the line segments annotated in the ShanghaiTech dataset as wireframe line segments. Wireframe line segments may be helpful for inferring 3D geometric information of the scene [12]. Motivated by the success of Convolutional Neural Networks (CNNs) for object detection and utilizing the dataset they created, DWP [12] trained a network to detect junctions and a network to detect line segments. Then the detected junctions and line segments are combined to produce the wireframe prediction. AFM [15] posed line segment detection as the region coloring problem by adopting a region-partition based attraction field representation of line segment maps. Leveraging the success of CNNs for semantic segmentation, it trained a model to predict the attraction field maps and then detected line segments from the computed attraction field maps using a squeeze module. L-CNN [13] first learns to detect junctions from the images, and then generate candidate line segments by learning the connectivities among junction proposals. Finally, candidate line segments are validated through a line verification module to get the predicted line segments. HAWP [17] adopts the same junction prediction and verification modules as L-CNN, but utilizes a different strategy to generate line segment proposals. Specifically, it adopts a geometric reparameterization for line segments and compute a 4-dimensional attraction field map for each image. The line segment candidates can then computed from the attraction field map. After generating the line segment proposals and junction proposals, they are matched and verified to get the final predictions. PPGNet [14] uses a convolutional neural network to infer the line segment graph which describes the junctions, line segments, and their relationships. LGNN [28] generates candidate line segments using a deep convolutional neural network, and utilizes a graph neural network to reason their connectivities. [29] shows that by adding geometric line priors with a trainable Hough transform block, the data efficiency of deep neural networks can be improved. TP-LSD [19] exploits a Tri-point based representation of line segments, and treats line segment detection as an end-to-end prediction of a root-point

and two endpoints. LETR [30] adapts the DETR [31] object detector for line segment detection by introducing a multi-scale encoder/decoder strategy, and a direct endpoint distance loss term in training, performing line segment detection in an end-to-end fashion using transformers. ELSD [20] proposes a one-stage architecture for line segment detection by representing a line segment using its center, angle, and length. F-Clip [32] proposes to represent line segments using their center, length, and angle, formulating the prediction of each parameter as a pixel-wise classification/regression problem. LSDNet [33] is built on top of the classical line segment detector LSD [9], by replacing the traditional gradient computation method with a light-weight convolutional neural network to leverage the efficiency of LSD. M-LSD [34] proposes a light-weight line segment detector on the basis of MobileNetV2 [35] for real-time line segment detection on computationally restricted and resource-constrained environments. HAWPv2 [18] is an improved version of HAWP [17], with a new method for binding line segment proposals and junction proposals. A new verification module is also introduced in HAWPv2. HAWPv3 [18] is a self-supervised model built on HAWPv2, which aims at improving the generalization capability for out-of-distribution images.

### C. Discussion on previous methods

Even though the efficiency of previous methods has been demonstrated in their specific domain, the performance of generic line segment detectors for the task of wireframe line segment detection won't be satisfactory, and vice versa. Besides, in the absence of a large dataset that can be used to train deep learning models for generic line segment detection, it is not easy to transfer the strategies adopted by most existing deep learning based wireframe line segment detectors to the task of generic line segment detection. In this paper, we propose a framework that can be used for both generic line segment detection and wireframe line segment detection, and show that it achieves state-of-the-art performance for both tasks. Details about the proposed method will be given in the next section.

## III. POEV2: A FLEXIBLE AND ROBUST FRAMEWORK FOR GENERIC LINE SEGMENT DETECTION AND WIREFRAME LINE SEGMENT DETECTION

Line segments are closely related to edge pixels in images: generic line segments correspond to straight parts of all meaningful edge pixels, while wireframe line segments correspond to straight parts of wireframe edge pixels. Therefore, line segment detection and edge detection are closely related tasks. For instance, Hough transform [6], [7], a famous line segment detector in the early stage, is designed to detect line segments from either binary edge maps or edge strength maps. Given an input image, an edge detector [22], [36] is first applied to detect edges in the image, and then Hough transform is applied to detect line segments. In other traditional line segment detectors, a gradient computation method is usually first applied to compute the edge strength map of the input image, and various strategies are then adopted to identify

the straight parts of edge pixels [9], [11]. Even though the accuracy of edge detection has been significantly boosted in recent years by deep learning based approaches [37], [38], [39], very few work studied on how to improve line segment detection accuracy leveraging a powerful edge detector. This phenomenon may be caused by the following reasons: first, the traditional way to detect line segments from binary edge maps if using Hough transform, while the performance of Hough transform is not satisfactory enough in many cases as discussed in [9], [11], [23], [21]; second, it is difficult to combine the edge grouping method adopted by traditional line segment detectors with deep learning based edge detectors, as the orientation of edge pixels is usually required while the deep learning based edge detectors compute only the edge strength map [9], [11], [21];

In [21], a Pixel Orientation Estimation (POE) based framework is proposed to detect line segments from binary edge maps, which aims at improving the line segment detection accuracy leveraging the progress made in edge detection by deep learning. Its efficiency was demonstrated for line segment detection in Synthetic Aperture Radar (SAR) images by combining it with a deep learning based edge detector for SAR images [36]. In this work, we show that by combining POE with an efficient edge detector for natural images, it achieves competitive performance for generic line segment detection, and achieves state-of-the-art performance for wireframe line segment detection. We also propose an improved version of POE, named as POEv2, and show that it sets new state-of-the-art for both generic line segment detection and wireframe line segment detection. In the following, we will describe the motivation and each part of POEv2 in detail.

#### A. Motivation

Similar to POE, the proposed POEv2 is proposed based on the following two intuitions: first, an edge pixel should have the same orientation as the line segment passing through it; second, when counting the number of edge pixels along different directions starting from an edge pixel, the maximum number of counts should occur along the direction of the line segment passing through it. Based on the above intuitions, the orientation of an edge pixel can be derived by identifying the direction that gives the maximum number of counts. After obtaining the orientations of edge pixels, candidate line segments can be obtained by a region growing algorithm which groups pixels sharing the same orientation.

Even though POE is efficient to detect line segments from binary edge maps, as shown in the experiments done in [21] and the experiments provided in Section IV, it can be improved in the following aspects:

- First, a binary edge map should be computed before applying POE. However, the outputs of recent deep learning based edge detectors are usually edge strength maps. A threshold has to be chosen to binarize the edge strength maps while very few work studies on how to set this threshold in general applications. The choice of this threshold influences heavily the performance of POE. When this threshold is set too high, many true edge pixels

will be discarded, leading to the missing of many true line segments. When this threshold is set low, POE may produce many false detections, as many false edge pixels are preserved.

- Second, the value of each pixel in the edge strength maps represents the probability of that pixel to be a true edge pixel. The higher the value of a pixel is, the more likely it is to be a true edge pixel. Therefore, more emphasis should be put on pixels with higher values, while POE treats all pixels equally.
- Third, the estimated orientation of each pixel can be used not only to group pixels sharing the same orientation, but also to guide the direction in which the region growing algorithm should go.

In the following, we will describe each part of POEv2 that takes the aforementioned aspects into account, resulting in a framework being less sensitive to the choice of threshold and more accurate.

#### B. Estimating pixel orientations from edge strength maps

Different from POE, the input of POEv2 is an edge strength map instead of a binary edge map. The edge strength map of a input image can be computed by any edge detector. The values of pixels in the edge strength map range between 0 and 1, where 1 indicates that the probability of this pixel to be an edge pixel is 100%, whereas 0 indicates that this pixel is definitely not an edge pixel.

For each pixel in the edge strength map with its value larger than 0, we compute the sum of pixel values along  $P$  directions. The direction that returns the maximum response is assumed to be the orientation of this pixel. Specifically, for a pixel  $u(x, y)$  located at  $(x, y)$  in the edge strength map  $u$ , the sum of pixel values is computed along  $P$  different directions. In the  $i$ -th direction ( $i = 1, 2, \dots, P$ ), the angle corresponding to this direction  $\theta_i$  is defined as  $\frac{(i-1)*\pi}{P}$ . The sum of pixel values in this direction can be computed as:

$$S_i(x, y) = \sum_{x'=-W}^W \sum_{y'=-W}^W u(x+x', y+y') \cdot Wt_i(x', y'), \quad (1)$$

where  $Wt_i(\cdot)$  is a regular-shaped window function corresponding to the  $i$ -th direction. The size of the window is  $(2 * W + 1) * (2 * W + 1)$  pixels, and the value of pixel located at  $(x', y')$  is set as follows:

$$Wt_i(x', y') = \begin{cases} 1.0 & \text{if } |-x' * \sin(\theta_i) + y' * \cos(\theta_i)| \\ & < 0.5 \text{ and } x'^2 + y'^2 \leq W^2, \\ 0.0 & \text{otherwise.} \end{cases} \quad (2)$$

After computing the sum of pixel values along all  $P$  directions, the angle corresponding to the direction that returns the maximum response is assumed to be the angle of the pixel located at  $(x, y)$ . In this paper,  $W$  is set to 7 and  $P$  is set to 16. More guidance about how to set these two parameters can be found in [21]. The maps of the 16 window functions can be found in Figure 1.

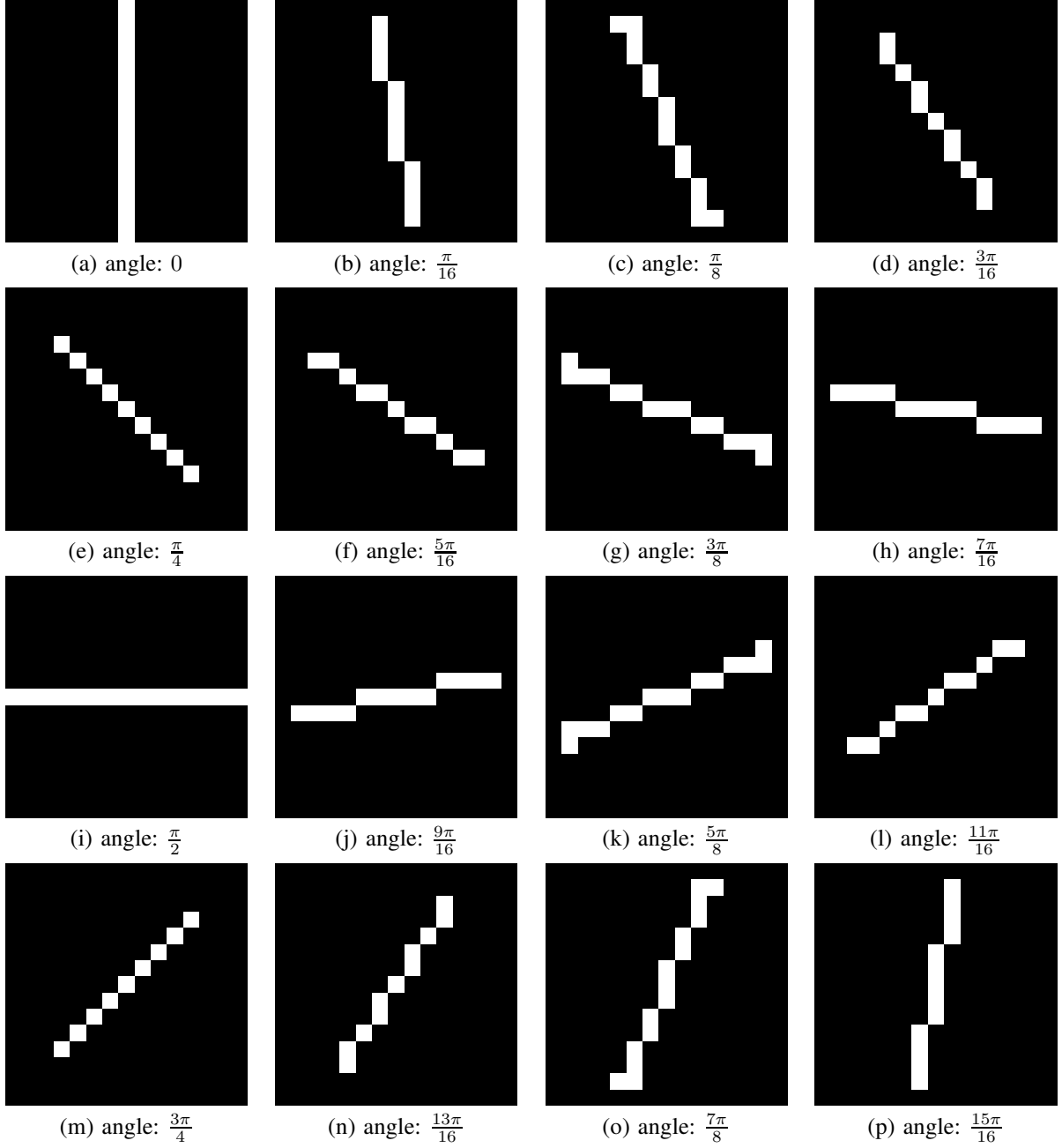


Fig. 1. The 16 window functions used to estimate the orientation of pixels.

### C. Guided Region Growing algorithm

After estimating the orientation of pixels with their values larger than 0 in the edge strength map, the next step is to group pixels belonging to the same line segment. As pixels with larger values are more likely to be true edge pixels, the region growing algorithm should start from pixels with larger values. We use a pseudo-ordering algorithm and put all the pixels in the edge strength map into 10 bins of equal width between 0 and 1 (the bins are  $(0, 0.1]$ ,  $(0.1, 0.2]$ ,  $\dots$ ,  $(0.9, 1.0]$ , respectively). The region growing algorithm visits these bins in descending order.

Since all the pixels belonging to the same line segment should have the same orientation as the line segment passing

through them, identifying the line segments in the image can thus be done by grouping pixels sharing the same orientations. Besides, the distances of all the pixels to their corresponding line segment should be less than 1 pixel in the ideal case, even in the presence of digitization effect of pixel locations in digital images. However, this constraint is too strong as many noisy pixels exist beside true edge pixels. The detected line segments may be fragmented and multiple line segments could be detected in the same location if this constraint is applied. Therefore, a line segment is represented by a region with certain width in this paper. During region growing, we require that the distance of the pixels in the region to their corresponding line segment should not be larger than  $l_w$  pixels. The value of  $l_w$  is chosen empirically from our experiment.

Choosing a large value may reduce the localization accuracy and angle accuracy of computed line segment as many noisy pixels far away from the line segment will be included into the region, whereas choosing a small value could lead to the problem of multiple responses and fragmented line segments. In our experiments, we find that setting  $l_w$  to 3 makes a good compromise. Consequently, the pixels in a region corresponding to a line segment are required to satisfy the following two constraints during region growing: first, the pixels should have the same orientation, up to an angle tolerance  $\tau$ ; second, the distance of these pixels to their corresponding line segment should not be larger than 3 pixels.

Starting from a pixel which is often called as the *seed pixel* of a region, the region growing algorithm searches in its  $s \times s$  neighborhood to see whether there are pixels can be added into the region. If a pixel is found to have the same angle as the seed pixel, and the distance of this pixel to the underlying line segment is not larger than 3 pixels, this pixel will be added into the region. The region growing algorithm will then search through the  $s \times s$  neighborhoods of all the pixels in the region to see whether there are pixels satisfying both constraints, and repeat this process until no pixel can be added into the region. Each time a pixel is added into the region, it will be labeled as *USED* and will not be visited again. When the searching process stops, a support region for a candidate line segment is formed. If the number of pixels in this region is equal to or larger than a threshold  $l_{min}$ , it will be accepted as the support regions of a true line segment and the endpoints of this line segment can be computed using the pixels in the region. If the number of pixels is smaller than  $l_{min}$ , this region will be discarded and all the pixels in the region will be labeled as *UNUSED* and can thus be visited again. Details about how to set  $l_{min}$  and how to compute the endpoints of a line segment given its support region will be discussed in subsequent subsections. After that, the region growing algorithm will start from another pixel having larger values until all the pixels in the edge strength map that can be considered as seed pixels are visited.

As all the pixels that can be added into a region are required to have the same orientation as the seed pixel of the region, it would be beneficial to require the seed pixel to satisfy a certain criterion. In our case, Only pixels with their values larger than  $\lambda$  can become seed pixels as they are more likely to be true edge pixels. This threshold is a bit similar to the one that is used to binarize a edge strength map. The difference is that the pixels with smaller values are all discarded during the process of binarization, while in our case these pixels will still be used to form support regions of possible line segments only if they satisfy both constraints required by a certain region. We will show in our experiments that the proposed POEv2 is much less sensitive to the choice of  $\lambda$  than POE, which uses  $\lambda$  to binarize edge strength maps.

The next question is how to compute the distance of a pixel to its corresponding line segment. Mathematically, the distance of a pixel to a line can be computed only if we know the coordinate of a pixel on the line and the angle of the line. Specifically, assuming a pixel located at  $(x_0, y_0)$  is on a line with angle  $\theta_0$ , then the distance of a pixel located at  $(x_1, y_1)$

to the line can be computed as:

$$|(x_1 - x_0) * \sin(\theta_0) + (y_1 - y_0) * \cos(\theta_0)|. \quad (3)$$

The chosen pixel on the line will be referred to as the *reference point* in this paper.

Initially, we have only a seed pixel in the region, and a line segment is expected to be found from this pixel through region growing. In this case, the seed pixel is chosen as the reference point, and its angle is chosen as the angle of the potential line passing through it. However, as we use discrete angles to approximate the angles of pixels in the edge strength map, a gap may exist between the estimated angle of a pixel and the angle of the line segment passing through it. Therefore, the angle of the potential line segment supported by the region should be updated when more pixels are added into the region, so is the location of the reference point. In our case, the angle of the potential line segment and the location of the reference point will be updated whenever the distance between a pixel added into the region and the reference point is larger than a certain threshold  $dist_r$ . This threshold should change whenever the line angle and reference point location are updated. The question is how to set and update  $dist_r$  properly.

Indeed, the line angle and reference point location are expected to become more accurate when they are updated. To achieve this goal, a sufficient number of pixels along the potential line segment must be contained in the region. Therefore, we would like to have as many pixels along the potential line segment added into the region as possible before updating the line angle and reference point location. We set  $dist_r$  according to the distance between the reference point and the farthest point along the potential line segment that can be reached by region growing when the difference between the current line angle and true line angle is maximum. Considering that we use  $P$  uniformly distributed discrete angles over  $[0, \pi)$  to estimate the angles of line segments in the image, the difference between the estimated line angle and real line angle should not be larger than  $\frac{\pi}{2*P}$ . Besides, an angle tolerance  $\tau$  is allowed when grouping pixels sharing the same angle as the seed pixel. A pixel can be added into the region if the angle difference between it and the seed pixel is not larger than  $\tau$ . As we set  $\tau$  to  $\frac{\pi}{P}$ , the difference between the angle of the seed pixel and the real line angle should not be larger than  $\frac{3*\pi}{2*P}$ . Therefore, the maximum possible angle difference should be  $\frac{3*\pi}{2*P}$ . In this case, the distance between the seed pixel and the farthest point along the potential line segment that can be reached by region growing can be computed as  $\frac{l_w}{\sin(\frac{3*\pi}{2*P})}$ . We set  $dist_r$  according to this value as follows:

$$dist_r = idx * \frac{l_w}{\sin(\frac{3*\pi}{2*P})}, \quad (4)$$

where  $idx$  is initially set to 1 and its value will be increased by 1 whenever the line angle and the reference point location are updated.

Now that we have determined the time that we should update the line angle and reference point location, the next question is how to update them. Initially, the seed pixel of

the region is chosen as the reference point and its angle is chosen as the line angle. As more and more pixels are added into the region, the reference point is updated as the center of the region and the line angle is updated as the angle between the horizontal axis and the first inertia axis of the region. The center of the region is defined as the center of mass, with the mass being the probabilities of pixels in the region to be true edge pixels.

Specifically, let  $(x(i), y(i))$  be the coordinate of the  $i$ -th pixel in the region, and let  $p(x(i), y(i))$  be the probability of it to be a true edge pixel, the coordinate of the region's center  $(c_x, c_y)$  can be computed as

$$c_x = \frac{\sum_{i \in \text{region}} p(x(i), y(i)) \cdot x(i)}{\sum_{i \in \text{region}} p(x(i), y(i))}, \quad (5)$$

$$c_y = \frac{\sum_{i \in \text{region}} p(x(i), y(i)) \cdot y(i)}{\sum_{i \in \text{region}} p(x(i), y(i))}. \quad (6)$$

The line angle can then approximated as the angle of the eigenvector corresponding to the smallest eigenvalue of the matrix

$$\mathbb{M} = \begin{pmatrix} \mathbb{M}^{xx} & \mathbb{M}^{xy} \\ \mathbb{M}^{xy} & \mathbb{M}^{yy} \end{pmatrix}, \quad (7)$$

where

$$\mathbb{M}^{xx} = \frac{\sum_{i \in \text{region}} p(x(i), y(i)) \cdot (x(i) - c_x)^2}{\sum_{i \in \text{region}} p(x(i), y(i))},$$

$$\mathbb{M}^{yy} = \frac{\sum_{i \in \text{region}} p(x(i), y(i)) \cdot (y(i) - c_y)^2}{\sum_{i \in \text{region}} p(x(i), y(i))},$$

and

$$\mathbb{M}^{xy} = \frac{\sum_{i \in \text{region}} p(x(i), y(i)) \cdot (x(i) - c_x) \cdot (y(i) - c_y)}{\sum_{i \in \text{region}} p(x(i), y(i))}.$$

Now we have known when and how to update the reference point location and line angle, the next question is how to set the size threshold  $l_{min}$ , which will be discussed in the next subsection.

#### D. Setting size threshold for computed regions

After region growing, a set of line support regions are obtained, whereas not all of them are corresponding to true line segments. We need to distinguish the regions supporting true line segments from those corresponding to false detections. Here we use the same strategy as POE and keeps only regions with their size larger than a size threshold  $l_{min}$ . This threshold  $l_{min}$  is defined as the size of *minimal meaningful line segment* according to the Helmholtz principle and the *a contrario* model [10], and can be computed as

$$l_{min} = \frac{\log(\varepsilon) - \log(N_L)}{\log(p)}, \quad (8)$$

where  $\varepsilon$  represents the number of false detections that is allowed,  $N_L$  represents the total number of possible line segments in a image, and  $p$  represents the probability that a pixel has the same angle as the line segment. In our case,  $\varepsilon$  is

set to 1,  $N_L$  is set to  $\sqrt{(M \cdot N)^5}$  for an image of size  $M \times N$  pixels, and  $p$  is set to  $\frac{3}{16}$  as we use 16 uniformly distributed discrete angles to estimate the angles of pixels and the angle tolerance  $\tau$  is chosen as  $\frac{\pi}{16}$ . More details about the definition of *minimal meaningful line segment*, the meaning of  $\varepsilon$ , and how to compute  $l_{min}$  can be found from [10], [9], [23], [21].

Only regions with their size larger than  $l_{min}$  are kept and the line segments they support are assumed to be correct detections. The question is how to compute the size of the region. In POE, the size of the region is simply defined as the number of pixels in the region. In our case, it is not appropriate to use this strategy as the probabilities of pixels in the region to be true edge pixels are different. Pixels with higher probabilities should contribute more to the size of the region than pixels with lower probabilities. In our case, the size of the region  $l_{region}$  is computed as

$$l_{region} = \sum_{i \in \text{region}} p_w(x(i), y(i)), \quad (9)$$

where

$$p_w(x(i), y(i)) = \begin{cases} 1.0 & \text{if } p(x(i), y(i)) \geq 0.3, \\ p(x(i), y(i)) & \text{otherwise,} \end{cases} \quad (10)$$

and  $p(x(i), y(i))$  represents the probability of the pixel located at  $(x(i), y(i))$  to be a true edge pixel. This setting aims at preserving as many true detections as possible while keeping the ability to reject false detections.

#### E. Computing the endpoints of detected line segments

As all the regions with their size larger than  $l_{min}$  are considered to support true line segments, the last question is how to derive the endpoints of line segments from these regions. Given a region, we can compute the center of the region and the angle of the line segment it supports in the same way as the one described in Subsection III-C. The center of the region can be regarded as the reference point on the line segment. Then, we can go through all the pixels in the region and compute the distances of them to the reference point along the direction of the line segment. After obtaining the largest distances of pixels to the reference point in the opposite direction along the line segment, the endpoints of the line segment can be easily computed by combining them with the reference point location and the angle of the line segment.

## IV. EXPERIMENTS

In this section, we will demonstrate the efficiency of the proposed POEv2 for both generic line segment detection and wireframe line segment detection. Specifically, we will compare the proposed method with existing line segment detectors in a generic line segment detection dataset, the YorkUrban-LineSegment dataset, which labels all the meaningful line segments in the images [11]; and a wireframe line segment detection dataset, the ShanghaiTech dataset, which labels the wireframe line segments in the images [12]. Similar to recent deep learning based wireframe line segment detectors, we also

compare the performance of the proposed method with existing ones in a Manhattan line segment detection dataset, the YorkUrban dataset [2], which labels only line segments satisfying the Manhattan assumption. The YorkUrban-LineSegment dataset is created from the YorkUrban dataset by labeling all the line segments in each image [11]. These two datasets share the same set of images just with different line segment annotations. Both of them contain 102 images of indoor and outdoor scenes from the campus of York University and downtown Toronto, Canada. The ShanghaiTech dataset contains 5462 images including both indoor and outdoor scenes of man-made environments. Among those images, 5000 images are used to train deep learning models and 462 images are used to compare the performance of different algorithms. We will compare the performance of POE, the proposed POEv2, with three state-of-the-art generic line segment detectors LSD [9], Linelet [11], DeepLSD [27], and two state-of-the-art wireframe line segment detectors HAWPv2 and HAWPv3 [18], using these three datasets. For LSD and Linelet, the default parameter settings are used. For DeepLSD, HAWPv2, and HAWPv3, we use the pre-trained weights provided by the authors, and the best results are reported.

#### A. Evaluation metrics

Most recent deep learning based wireframe line segment detectors exploit Structural Average Precision (sAP, also known as Structural AP) to compare the performance of different methods on the ShanghaiTech dataset and the YorkUrban dataset. We argue that this metric puts too much emphasis on the completeness and connectivity of line segments, while the localization accuracy of them is not guaranteed. Indeed, the localization accuracy of line segments is much more important than their completeness and connectivity. For instance, the junctions' location can be accurately derived if the detected line segments have good localization accuracy, even if they are not complete and not connected with each other. In the following, we will explain why Structural AP is not suitable for evaluating the efficiency of a line segment detector.

Structural AP is first proposed in [13]. It is defined as the area under the precision-recall curve computed from the detected line segments on all test images. The detected line segments are ranked according to the confidence scores computed by a learned verification module. Precision is computed as the proportion of correctly detected line segments to all detections, up to a certain cutoff score. Recall is computed as the proportion of correctly detected line segments to all ground truth line segments, up to the same cutoff score. In this procedure, a line segment  $L_j = (p_j^1, p_j^2)$  is considered to be correctly detected if and only if

$$\min_{(p_m, p_n) \in \mathcal{L}_{gt}} \|p_j^1 - p_m\|_2^2 + \|p_j^2 - p_n\|_2^2 \leq d_{threshold}, \quad (11)$$

where  $\mathcal{L}_{gt}$  represents the set of ground truth line segments in the image.  $p_m$  and  $p_n$  represent the endpoint coordinates of a ground truth line segment, with  $(m, n)$  being either  $(1, 2)$  or  $(2, 1)$ .  $d_{threshold}$  determines the strictness of the metric. Each ground truth line segment is allowed to be matched at most once so as to penalize multiple detections of a line segment.

In previous works,  $d_{threshold}$  is often set to 5, 10, and 15, under the resolution  $128 \times 128$ . The computed Structural AP is abbreviated as sAP<sup>5</sup>, sAP<sup>10</sup>, and sAP<sup>15</sup>, respectively. However, the line segments satisfying the constraint defined in (11) may have poor localization accuracy, while they will be considered as correct detections. For instance, assuming that the line segment  $L_j$  matches with the ground truth line segment  $(p_1, p_2)$ , and  $p_j^1 - p_1 = 0$ , then only if  $\|p_j^2 - p_2\|_2^2 \leq d_{threshold}$ ,  $L_j$  will be considered as a correct detection. This means that one endpoint of a detected line segment can deviate from the endpoint of the ground truth line segment it matches for up to  $\sqrt{d_{threshold}}$  pixels. In the strictest situation, the deviation can be up to  $\sqrt{5}$  pixels under the resolution  $128 \times 128$ , which means that under the image resolution  $512 \times 512$ , the deviation can be up to  $\sqrt{80}$  pixels. If this deviation is in the direction perpendicular to the direction of the ground truth line segment, the angle of the detected line segment will differ a lot from that of the ground truth line segment. It should be considered as a false detection, but it is considered as a correct detection following the criterion of sAP<sup>5</sup>.

From the above points, we argue that Structural AP can not fully represent the accuracy of detected line segments, and is thus not appropriate for evaluating the performance of line segment detectors. Therefore, we will use the heat map based metric, a metric that is also widely used in recent line segment detectors, to compare the performance of different methods.

During evaluation, a binary line segment map is obtained by rasterizing all detected line segments, where the value of a pixel in the line segment map is set to 1 if it belongs to a certain detected line segment, and set to 0 otherwise. This line segment map is compared to the ground truth line segment map, which is obtained by rasterizing all the ground truth line segments, to evaluate the accuracy of detection. Given the detected line segment map and the ground truth line segment map, an F1-score (also known as  $F^H$  in previous works) can be computed as

$$F^H = \frac{2 * precision * recall}{precision + recall}, \quad (12)$$

where *precision* is computed as the proportion of correctly detected line segment pixels to all detected line segment pixels, and *recall* is computed as the proportion of correctly detected line segment pixels to all ground truth line segment pixels. Average Precision (AP<sup>H</sup>) and Average Recall (AR<sup>H</sup>) are also reported to compare the performance of different algorithms from different aspects.

#### B. Edge detection algorithms

Similar to POE and Hough transform, the proposed POEv2 is designed to be combined with an edge detector so as to perform line segment detection in images. Indeed, the step of edge detection can be done by any edge detector. In this paper, we use EdgeNAT [39], a transformer based edge detector that is built on the basis of the Dilated Neighborhood Attention Transformer (DiNAT) [40], due to its efficiency for edge detection. For generic line segment detection, edgeNAT is trained on the BIPEDv2 dataset [41], which labels all



the meaningful edges in the images. The data augmentation strategy provided by the authors is used. For wireframe line segment detection and Manhattan line segment detection, EdgeNAT is trained using the training set of the ShanghaiTech dataset. As the annotations in the ShanghaiTech dataset are wireframe line segments and not wireframe edges, the line segment annotations are transformed into line segment maps (refer to Subsection IV-A for more details). The obtained line segment maps are wireframe edge maps. During training, the training images and their corresponding wireframe edge maps are first flipped horizontally, vertically and both. They are then rescaled to five different scales, 50%, 80%, 100%, 120%, and 150%.

We use a PyTorch implementation of EdgeNAT, and train it using the AdamW optimizer. The weighted cross entropy loss is used as the loss function. The pre-trained weights of DiNAT [40] on the ImageNet-22K dataset [42] are used to initialize the parameter values of EdgeNAT. During training, the learning rate, mini-batch size for training, and weight decay are set to  $6 \times 10^{-5}$ , 8, and 0.01 respectively. The models are trained for 15 epochs and the checkpoints that produce the best edge detection results are kept.

During prediction, a multi-scale testing technique [39] is exploited to get better edge detection results. Standard Non-Maxima Suppression [43] is applied to obtain thinned edge strength maps. For POE, a threshold  $\lambda$  is used to binarize the edge strength maps, where the value of a pixel is set to 0 if its value is not larger than  $\lambda$ , and set to 1 otherwise. For POEv2, a similar threshold is used, but the purpose of it is to determine whether a pixel can serve as the seed pixel during region growing. It is also notated as  $\lambda$  for simplicity. We will study the influence of  $\lambda$  on the performance of POE and POEv2 in subsequent subsection.

### C. Parameter settings of POE and POEv2

For both POE and POEv2, the size of the window function is  $(2*W+1)*(2*W+1)$  pixels with  $W = 7$ . The number of discrete angles  $P$  is set to 16, and the angle tolerance  $\tau$  is set to  $\frac{\pi}{16}$ . For POEv2, the distance threshold  $l_w$  is set to 3. Here we will study the influence of the following two parameters on the performance of POE and POEv2: the threshold  $\lambda$ , which is used to process the edge strength maps; and the searching neighborhood size  $s \times s$ , which is used during region growing.

1) *Influence of  $\lambda$  on the performance of POE and POEv2:* As POE and POEv2 should be combined with edge detectors to perform line segment detection, a threshold  $\lambda$  is required to process the edge strength maps. For POE,  $\lambda$  is used for binarization, while for POEv2,  $\lambda$  is used to determine whether a pixel can serve as the seed pixel during region growing. Here we study the influence of  $\lambda$  on the performance of both methods on the YorkUrban-LineSegment dataset and the ShanghaiTech dataset, by setting  $\lambda$  to 10 different values. The searching neighborhood size is set to  $5 \times 5$  for the YorkUrban-LineSegment dataset, and is set to  $3 \times 3$  for the ShanghaiTech dataset. The  $F^H$  computed by both methods on the YorkUrban-LineSegment dataset and the ShanghaiTech dataset are displayed in Table I and Table II, respectively. It

is clearly shown in both tables that the performance of the proposed POEv2 is much less sensitive to the choice of  $\lambda$ , and POEv2 achieves consistently better performance than POE in all the values of  $\lambda$ . The best scores obtained by POEv2 is around 1.6 percent higher than that obtained by POE on the YorkUrban-LineSegment dataset, and around 1.9 percent higher than that obtained by POE on the ShanghaiTech dataset. Besides, it can be seen from Table I that for generic line segment detection, smaller values of  $\lambda$  are preferred. This could be because the aim is to detect as many meaningful line segments in the images as possible. While for wireframe line segment detection, larger values of  $\lambda$  are preferred, as the aim is to detect only line segments corresponding to scene structures.

2) *Influence of searching neighborhood size  $s \times s$  on the performance of POE and POEv2:* During region growing, both methods search in the  $s \times s$  neighborhood of pixels in the region to see whether other pixels can be added into the region. Here we study the influence of searching neighborhood size on the performance of POE and POEv2. For the experiments on the YorkUrban-LineSegment dataset,  $\lambda$  is set to 0.1 for both methods. For the experiments on the ShanghaiTech dataset,  $\lambda$  is set to 0.5 for POE, and is set to 0.8 for POEv2. The values of  $\lambda$  are chosen according to the results displayed in Table I and Table II.

The  $F^H$  computed by both methods with several searching neighborhood sizes on the YorkUrban-LineSegment dataset and the ShanghaiTech dataset are displayed in Table III and Table IV, respectively. It can be seen from both tables that the proposed POEv2 obtains consistently higher scores than POE in all these experiments. On the YorkUrban-LineSegment dataset, the score computed by POEv2 becomes higher as the size of searching neighborhood increases, while the score computed by POE is the highest when searching neighborhood size is  $5 \times 5$ . On the ShanghaiTech dataset, the score computed by both methods does not change a lot when the size of searching neighborhood changes. Besides, the highest score computed by POEv2 is around 3.6 percent higher than the highest score computed by POE on the YorkUrban-LineSegment dataset, and is around 1.9 percent higher than that computed by POE on the ShanghaiTech dataset.

### D. Comparison with state-of-the-art on the YorkUrban-LineSegment dataset

In this part, we compare the performance of different methods for generic line segment detection. Three state-of-the-art generic line segment detectors (LSD, Linelet, DeepLSD) and two state-of-the-art wireframe line segment detectors (HAWPv2, HAWPv3) are chosen to compare with the performance of POE and POEv2. For POE and POEv2,  $\lambda$  is set to 0.1. For POE, the searching neighborhood size is set to  $5 \times 5$  as it achieves the highest score on the YorkUrban-LineSegment dataset with this choice, as shown in Table III. For POEv2, the searching neighborhood size is set to  $5 \times 5$ ,  $7 \times 7$ , and  $15 \times 15$ . POEv2 with these searching neighborhood sizes are denoted as POEv2 $_{5 \times 5}$ , POEv2 $_{7 \times 7}$ , and POEv2 $_{15 \times 15}$ , respectively. The  $AP^H$ ,  $AR^H$ , and  $F^H$  computed by different methods on the YorkUrban-LineSegment dataset are displayed in Table V.

TABLE I  
INFLUENCE OF  $\lambda$  ON THE PERFORMANCE OF POE AND POEv2 ON THE YORKURBAN-LINESEGMENT DATASET.

| $\lambda$     | 0.0    | 0.1    | 0.2    | 0.3    | 0.4    | 0.5    | 0.6    | 0.7    | 0.8    | 0.9    |
|---------------|--------|--------|--------|--------|--------|--------|--------|--------|--------|--------|
| $F^H$ (POE)   | 0.8234 | 0.8308 | 0.8273 | 0.8230 | 0.8153 | 0.8052 | 0.7886 | 0.7567 | 0.6047 | 0.0449 |
| $F^H$ (POEv2) | 0.8467 | 0.8468 | 0.8466 | 0.8467 | 0.8464 | 0.8450 | 0.8426 | 0.8381 | 0.8294 | 0.7729 |

TABLE II  
INFLUENCE OF  $\lambda$  ON THE PERFORMANCE OF POE AND POEv2 ON THE SHANGHAI TECH DATASET.

| $\lambda$     | 0.0    | 0.1    | 0.2    | 0.3    | 0.4    | 0.5    | 0.6    | 0.7    | 0.8    | 0.9    |
|---------------|--------|--------|--------|--------|--------|--------|--------|--------|--------|--------|
| $F^H$ (POE)   | 0.7750 | 0.8323 | 0.8417 | 0.8472 | 0.8510 | 0.8531 | 0.8522 | 0.8493 | 0.8404 | 0.7951 |
| $F^H$ (POEv2) | 0.8590 | 0.8590 | 0.8591 | 0.8597 | 0.8632 | 0.8669 | 0.8697 | 0.8716 | 0.8720 | 0.8674 |

TABLE III  
INFLUENCE OF THE SEARCHING NEIGHBORHOOD SIZE ON THE PERFORMANCE OF POE AND POEv2 ON THE YORKURBAN-LINESEGMENT DATASET.

| $s \times s$  | $3 \times 3$ | $5 \times 5$ | $7 \times 7$ | $11 \times 11$ | $15 \times 15$ |
|---------------|--------------|--------------|--------------|----------------|----------------|
| $F^H$ (POE)   | 0.8197       | 0.8308       | 0.7988       | 0.6934         | 0.5873         |
| $F^H$ (POEv2) | 0.8209       | 0.8468       | 0.8535       | 0.8619         | 0.8665         |

TABLE IV  
INFLUENCE OF THE SEARCHING NEIGHBORHOOD SIZE ON THE PERFORMANCE OF POE AND POEv2 ON THE SHANGHAI TECH DATASET.

| $s \times s$  | $3 \times 3$ | $5 \times 5$ | $7 \times 7$ |
|---------------|--------------|--------------|--------------|
| $F^H$ (POE)   | 0.8531       | 0.8499       | 0.8440       |
| $F^H$ (POEv2) | 0.8720       | 0.8722       | 0.8712       |

TABLE V  
QUANTITATIVE COMPARISONS OF DIFFERENT ALGORITHMS ON THE YORKURBAN-LINESEGMENT DATASET.

| Methods                 | $AP^H$ | $AR^H$ | $F^H$  |
|-------------------------|--------|--------|--------|
| LSD [9]                 | 0.9077 | 0.7354 | 0.8125 |
| Linelet [11]            | 0.8595 | 0.8428 | 0.8511 |
| DeepLSD [27]            | 0.8818 | 0.7708 | 0.8226 |
| HAWPv2 [18]             | 0.8278 | 0.7112 | 0.7651 |
| HAWPv3 [18]             | 0.4930 | 0.8461 | 0.6230 |
| POE [21]                | 0.9145 | 0.7611 | 0.8308 |
| POEv2 $_{5 \times 5}$   | 0.9277 | 0.7788 | 0.8468 |
| POEv2 $_{7 \times 7}$   | 0.9209 | 0.7952 | 0.8535 |
| POEv2 $_{15 \times 15}$ | 0.8960 | 0.8389 | 0.8665 |

From Table V we can see that the highest  $F^H$  obtained by previous methods is 0.8511 done by Linelet, which is around 1.6 percent lower than the one computed by the proposed POEv2 with searching neighborhood size set to  $15 \times 15$ . However, the  $AP^H$  computed by Linelet is much lower than those computed by other generic line segment detectors, which means that it produces more false detections. The  $F^H$  computed by DeepLSD is lower than that computed by Linelet, but its  $AP^H$  is around 2 percent higher than that of Linelet. Among the previous methods, POE reports the highest score in terms of  $AP^H$ , and the second highest score in terms of  $F^H$ . The scores computed by HAWPv2 and HAWPv3 are much lower than other methods, which can be expected as they are trained to detect wireframe line segments in images.

For the proposed POEv2, it achieves the highest score in terms of  $F^H$  when the searching neighborhood size is set to  $15 \times 15$ . However, the  $AP^H$  computed by POEv2 $_{15 \times 15}$  is lower than those computed by LSD, POE, POEv2 $_{5 \times 5}$ , and POEv2 $_{7 \times 7}$ . Therefore, POEv2 $_{15 \times 15}$  is not recommended for general applications because it produces more false detections. In comparison, POEv2 $_{5 \times 5}$  and POEv2 $_{7 \times 7}$  are better choices as the  $AP^H$  computed by them are higher than other methods. Besides, the  $F^H$  computed by POEv2 $_{7 \times 7}$  is higher than previous state-of-the-art, and the  $F^H$  computed by POEv2 $_{5 \times 5}$  is only slightly lower than the previous highest score.

The line segment detection results on an image of the YorkUrban-LineSegment dataset computed by LSD, Linelet, DeepLSD, HAWPv2, POE, POEv2 $_{5 \times 5}$ , and POEv2 $_{7 \times 7}$  are displayed in Figure 2. The result computed by HAWPv3 is not provided due to the low scores computed by it. Even though POEv2 $_{15 \times 15}$  achieves the highest  $F^H$ , the result computed by it is also not provided due to its relative low  $AP^H$ . POEv2 $_{5 \times 5}$  and POEv2 $_{7 \times 7}$  are better choices for general use as they produce fewer false detections. It can be seen from Figure 2 that the line segments detected by LSD and Linelet tend to be fragmented. Some line segments may not be detected by LSD while Linelet produces many false detections. Compared to them, the line segments computed by DeepLSD are more complete. However, DeepLSD detects fewer true line segments and it produces overlapping line segments in some places. As HAWPv2 is trained to detect only wireframe line segments, many true line segments are missing by it. Besides, it produces many false line segments which may be caused by its poor generalization capability. Moreover, the endpoints of many line segments are falsely connected, which may be because it emphasizes the completeness and connectivity of line segments. POE detects fewer true line segments than DeepLSD, but it produces fewer false detections and it rarely produces overlapping line segments. Similar to POE, POEv2 detects much fewer false line segments than other methods, and it

detects more true line segments than POE. All in all, POEv2 produces the best line segment detection results taking into account of line segment completeness, detection capability, and false detection control ability.

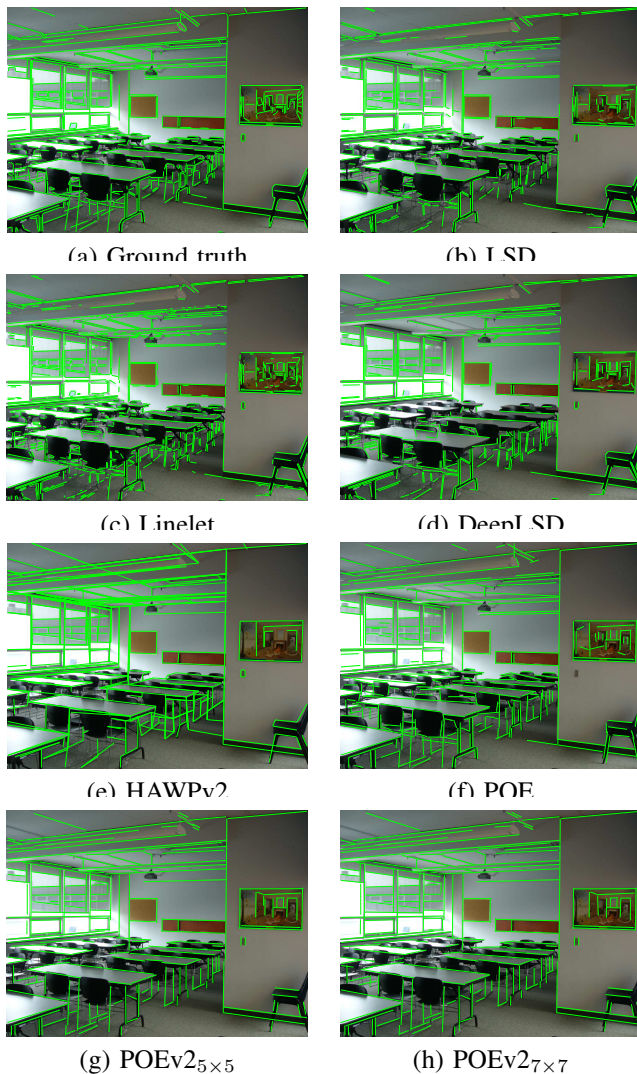


Fig. 2. Line segment detection results computed by different methods on an image from the YorkUrban-LineSegment dataset.

#### E. Comparison with state-of-the-art on the ShanghaiTech dataset

In this part, we demonstrate the efficiency of the proposed POEv2 for wireframe line segment detection, by comparing it with other methods on the ShanghaiTech dataset. The searching neighborhood size is set to  $3 \times 3$  for POE and POEv2.  $\lambda$  is set to 0.5 for POE. For POEv2,  $\lambda$  is set to 0.8 and 0.9. The  $AP^H$ ,  $AR^H$ , and  $F^H$  computed by different methods are displayed in Table VI, where \* indicates that the scores computed by the method are extracted from the paper of HAWPv2.

It is clearly shown in Table VI that the scores computed by the generic line segment detectors (LSD, Linelet, and DeepLSD) are much lower than those computed by recent wireframe line segment detectors. This can be expected as

TABLE VI  
QUANTITATIVE COMPARISONS OF DIFFERENT ALGORITHMS ON THE SHANGHAITECH DATASET. \* INDICATES THAT THE SCORES COMPUTED BY THE METHOD ARE EXTRACTED FROM THE PAPER OF HAWPv2.

| Methods                   | $AP^H$ | $AR^H$ | $F^H$  |
|---------------------------|--------|--------|--------|
| LSD [9]                   | 0.4993 | 0.8502 | 0.6291 |
| Linelet [11]              | 0.4499 | 0.89   | 0.5977 |
| DeepLSD [27]              | 0.4817 | 0.8527 | 0.6156 |
| DWP* [12]                 | 0.678  | -      | 0.722  |
| AFM* [15]                 | 0.692  | -      | 0.772  |
| AFM++* [16]               | 0.748  | -      | 0.828  |
| L-CNN* [13]               | 0.816  | -      | 0.779  |
| F-Clip* (HG2-LB) [32]     | 0.851  | -      | 0.809  |
| LETR* (R101) [30]         | 0.855  | -      | 0.798  |
| LETR* (R50) [30]          | 0.847  | -      | 0.791  |
| ELSD* (HG) [20]           | 0.847  | -      | 0.803  |
| ELSD* (Res34) [20]        | 0.872  | -      | 0.823  |
| HAWPv1* [17]              | 0.845  | -      | 0.803  |
| HAWPv2* [18]              | 0.880  | -      | 0.814  |
| HAWPv2 [18]               | 0.8489 | 0.7828 | 0.8145 |
| HAWPv3 [18]               | 0.5899 | 0.7024 | 0.6413 |
| POE [21]                  | 0.8399 | 0.8668 | 0.8531 |
| POEv2 ( $\lambda = 0.8$ ) | 0.8642 | 0.88   | 0.8720 |
| POEv2 ( $\lambda = 0.9$ ) | 0.8853 | 0.8502 | 0.8674 |

the aim of LSD, Linelet, and DeepLSD is to detect all the meaningful line segments in the images, many of which will be considered as False detections in the case of wireframe line segment detection. For HAWPv2, the scores computed by our evaluation are different from the scores provided in the paper, with lower  $AP^H$  score but similar  $F^H$ . The scores computed by HAWPv3 are surprisingly low, which may be caused by the fact that it exploits a self-supervised training strategy. Notice that we adopted the official implementations of HAWPv2 and HAWPv3, and used the pre-trained weights provided by the author. We have tried our best to optimize their performance, and therefore believe that we have evaluated their performance appropriately and sufficiently.

In comparison, by combining POE and POEv2 with a wireframe edge detector, both of them achieves higher  $F^H$  scores than previous wireframe line segment detectors. When  $\lambda$  is set to 0.9, POEv2 achieves higher scores in all three criteria than previous methods, showing its stronger detection capability and false detection control ability. In particular, the  $F^H$  scores computed by POEv2 are at least 1.4 percent higher than POE, and at least 3.9 percent higher than previous deep learning based wireframe line segment detectors. Besides, the  $AP^H$  scores computed by POEv2 are at least 2.4 percent higher than POE, showing that POEv2 has strong capabilities to control the number of false detections.

The line segment detection results computed by LSD, DeepLSD, HAWPv2, POE, and POEv2 on an image from the ShanghaiTech dataset can be found in Figure 3. It can

be seen from Figure 3 that LSD and DeepLSD are not able to distinguish between wireframe line segments and other line segments. Compared to LSD and DeepLSD, the line segment detection result computed by HAWPv2 is better as it produces fewer false detections. Besides, the completeness and connectivity of line segments detected by HAWPv2 are the best among these approaches. However, it may produce false connections among the endpoints of line segments, which reduces the reliability of it. In comparison, POE and POEv2 detect more true line segments than HAWPv2, but they also produce more false detections. The detection capability of POE and POEv2 are similar, but POEv2's ability to control the number of false detections is stronger.

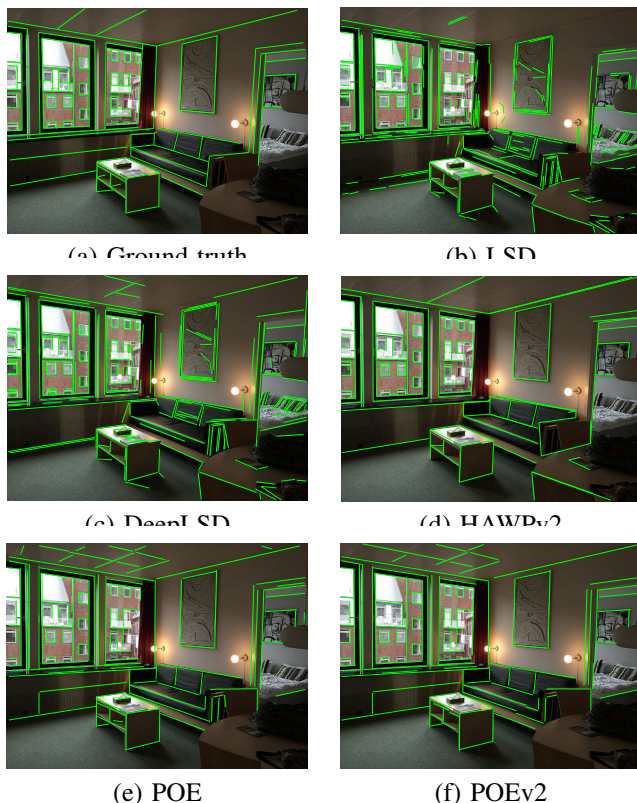


Fig. 3. Line segment detection results computed by different methods on an image from the ShanghaiTech dataset.

#### F. Comparison with state-of-the-art on the YorkUrban dataset

Indeed, the detection of line segments on the YorkUrban dataset is a different task from generic line segment detection and wireframe line segment detection. Only line segments that satisfy the Manhattan assumption are labeled on the YorkUrban dataset, while almost none of recent deep learning methods is designed for this purpose. Despite this, we also provide comparisons of different methods on the YorkUrban dataset. The parameter setting of POE and POEv2 are different from those in previous experiments. The fewer line segments they detect, the higher scores they obtain. Therefore,  $\lambda$  is set to 0.9 and the searching neighborhood size is set to  $3 \times 3$  for both methods. Besides, unlike previous settings in POEv2, pixels whose values are not larger than  $\lambda$  are discarded as the aim is to detect as few line segments as possible.

TABLE VII  
QUANTITATIVE COMPARISONS OF DIFFERENT ALGORITHMS ON THE YORKURBAN DATASET. \* INDICATES THAT THE SCORES COMPUTED BY THE METHOD ARE EXTRACTED FROM THE PAPER OF HAWPv2.

| Methods               | AP <sup>H</sup> | AR <sup>H</sup> | F <sup>H</sup> |
|-----------------------|-----------------|-----------------|----------------|
| LSD [9]               | 0.4333          | 0.8938          | 0.5837         |
| Linelet [11]          | 0.3784          | 0.9397          | 0.5395         |
| DeepLSD [27]          | 0.4054          | 0.9013          | 0.5592         |
| DWP* [12]             | 0.510           | -               | 0.616          |
| AFM* [15]             | 0.482           | -               | 0.633          |
| AFM++* [16]           | 0.505           | -               | 0.668          |
| L-CNN* [13]           | 0.583           | -               | 0.622          |
| F-Clip* (HG2-LB) [32] | 0.623           | -               | 0.645          |
| LETR* (R101) [30]     | 0.596           | -               | 0.620          |
| LETR* (R50) [30]      | 0.617           | -               | 0.634          |
| ELSD* (HG) [20]       | 0.578           | -               | 0.621          |
| ELSD* (Res34) [20]    | 0.620           | -               | 0.636          |
| HAWPv1* [17]          | 0.606           | -               | 0.648          |
| HAWPv2* [18]          | 0.646           | -               | 0.645          |
| HAWPv2 [18]           | 0.6401          | 0.7057          | 0.6713         |
| HAWPv3 [18]           | 0.5241          | 0.6244          | 0.5699         |
| POE [21]              | 0.6465          | 0.81217         | 0.7199         |
| POEv2                 | 0.6516          | 0.8291          | 0.7297         |

It can be seen from Table VII that the F<sup>H</sup> computed by POE and POEv2 are much higher than those computed by previous methods. Compared to POE, the scores computed by POEv2 are higher, setting new state-of-the-art for Manhattan line segment detection. However, it should be noted that the reliable detection of Manhattan line segments requires a dataset large enough for training.

The line segment detection results computed by different methods on an image from the YorkUrban dataset can be found in Figure 4. Again, the performance of LSD and DeepLSD are not satisfactory. Many line segments detected by them will be considered as false detections in the case of Manhattan line segment detection. The performance of HAWPv2 is better as it detects fewer line segments. However, the angles of some line segments detected by HAWPv2 may not be that accurate. All in all, the results computed by POE and POEv2 are closer to the ground truth, as they detect more true line segments and produce fewer false detections.

#### V. CONCLUSIONS

In this paper, we study the problem of line segment detection in images. Unlike most previous methods that can be used for only either generic line segment detection or wireframe line segment detection, the proposed POEv2 can be used for both and is thus more flexible. Besides, the proposed POEv2 detects line segments from edge strength maps, and can thus be combined with any edge detector, which means that any progress made in edge detection can be easily transferred to line segment detection by the proposed method.



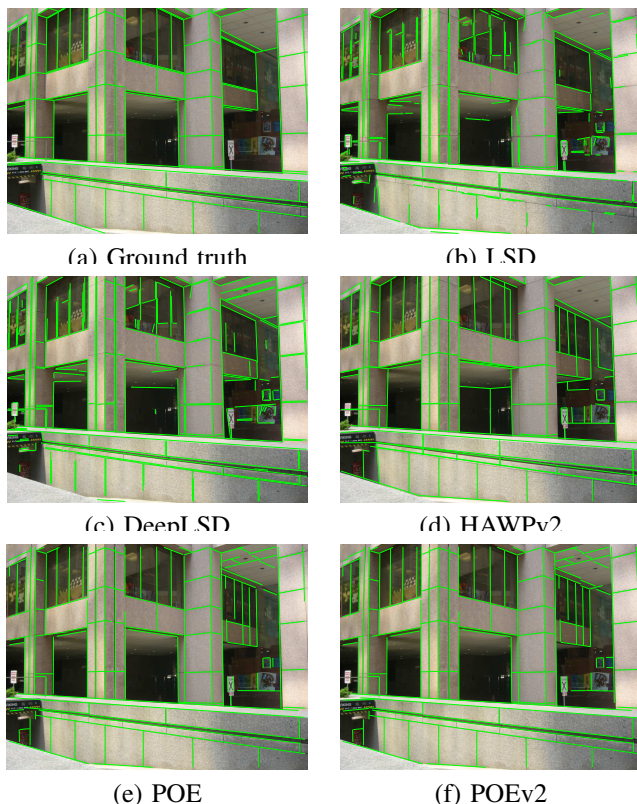


Fig. 4. Line segment detection results computed by different methods on an image from the YorkUrban dataset.

Comprehensive experiments demonstrate the efficiency of the proposed method.

## FUNDINGS

This work is supported in part by the National Natural Science Foundation of China (Grant No. 42374018 and Grant No. 42304012), in part by the Guangdong Basic and Applied Basic Research Foundation (Grant No. 2025B1515020092 and Grant No. 2022A1515110730), and in part by the Shenzhen Science and Technology Program (Grant No. KCXFZ20240903093000002 and Grant No. JCYJ20220531101409021).

## VI. REFERENCES

### REFERENCES

- [1] J. Lezama, R. G. von Gioi, G. Randall, and J.-M. Morel, "Finding vanishing points via point alignments in image primal and dual domains," in *2014 IEEE Conference on Computer Vision and Pattern Recognition*, 2014, pp. 509–515.
- [2] P. Denis, J. H. Elder, and F. J. Estrada, "Efficient edge-based methods for estimating manhattan frames in urban imagery," in *European Conference on Computer Vision*, 2008, pp. 197–210.
- [3] P. Arbelaez, M. Maire, C. Fowlkes, and J. Malik, "Contour detection and hierarchical image segmentation," *IEEE Transactions on Pattern Analysis and Machine Intelligence*, vol. 33, pp. 898–916, 2011.
- [4] A. Y.-S. Chia, D. Rajan, M. K. Leung, and S. Rahardja, "Object recognition by discriminative combinations of line segments, ellipses, and appearance features," *IEEE Transactions on Pattern Analysis and Machine Intelligence*, vol. 34, pp. 1758–1772, 2012.
- [5] Z. Yu, X. Guo, H. Ling, A. Lumsdaine, and J. Yu, "Line assisted light field triangulation and stereo matching," in *2013 IEEE International Conference on Computer Vision*, 2013, pp. 2792–2799.

- [6] R. O. Duda and P. E. Hart, "Use of the hough transformation to detect lines and curves in pictures," *Communications of the ACM*, vol. 15, pp. 11–15, 1972.
- [7] J. Skingley and A. J. Rye, "The hough transform applied to sar images for thin line detection," *Pattern Recognition Letters*, vol. 6, pp. 61–67, 1987.
- [8] J. B. Burns, A. R. Hanson, and E. M. Riseman, "Extracting straight lines," *IEEE Transactions on Pattern Analysis and Machine Intelligence*, vol. PAMI-8, no. 4, pp. 425–455, 1986.
- [9] R. Grompone von Gioi, J. Jakubowicz, J.-M. Morel, and G. Randall, "Lsd: A fast line segment detector with a false detection control," *IEEE Transactions on Pattern Analysis and Machine Intelligence*, vol. 32, pp. 722–732, 2010.
- [10] A. Desolneux, L. Moisan, and J.-M. Morel, "Meaningful alignments," *International Journal of Computer Vision*, vol. 40, pp. 7–23, 2000.
- [11] N.-G. Cho, A. Yuille, and S.-W. Lee, "A novel linelet-based representation for line segment detection," *IEEE Transactions on Pattern Analysis and Machine Intelligence*, vol. 40, pp. 1195–1208, 2018.
- [12] K. Huang, Y. Wang, Z. Zhou, T. Ding, S. Gao, and Y. Ma, "Learning to parse wireframes in images of man-made environments," in *The IEEE Conference on Computer Vision and Pattern Recognition (CVPR)*, 2018.
- [13] Y. Zhou, H. Qi, and Y. Ma, "End-to-End Wireframe Parsing," in *IEEE Conference on Computer Vision (ICCV) 2019*, 2019.
- [14] Z. Zhang, Z. Li, N. Bi, J. Zheng, J. Wang, K. Huang, W. Luo, Y. Xu, and S. Gao, "PPGNet: Learning Point-Pair Graph for Line Segment Detection," in *2019 IEEE/CVF Conference on Computer Vision and Pattern Recognition (CVPR)*, 2019.
- [15] N. Xue, S. Bai, F. Wang, G. Xia, T. Wu, and L. Zhang, "Learning attraction field representation for robust line segment detection," in *Proceedings of the IEEE Conference on Computer Vision and Pattern Recognition*, 2019, pp. 1595–1603.
- [16] N. Xue, S. Bai, F.-D. Wang, G.-S. Xia, T. Wu, L. Zhang, and P. H. Torr, "Learning regional attraction for line segment detection," *IEEE Transactions on Pattern Analysis and Machine Intelligence*, vol. 43, pp. 1998–2013, 2021.
- [17] N. Xue, T. Wu, S. Bai, F.-D. Wang, G.-S. Xia, L. Zhang, and P. H. S. Torr, "Holistically-attracted wireframe parsing," in *IEEE Conference on Computer Vision and Pattern Recognition (CVPR)*, 2020.
- [18] —, "Holistically-attracted wireframe parsing: From supervised to self-supervised learning," *IEEE Transactions on Pattern Analysis and Machine Intelligence*, vol. 45, pp. 14 727–14 744, 2023.
- [19] S. Huang, F. Qin, P. Xiong, N. Ding, Y. He, and X. Liu, "Tp-lsd: Tri-points based line segment detector," in *European Conference on Computer Vision*, 2020, pp. 770–785.
- [20] H. Zhang, Y. Luo, F. Qin, Y. He, and X. Liu, "Elsd: Efficient line segment detector and descriptor," in *2021 IEEE/CVF International Conference on Computer Vision (ICCV)*, 2021, pp. 2949–2958.
- [21] C. Liu, C. Liu, C. Wang, W. Zhu, and Q. Li, "A novel pixel orientation estimation based line segment detection framework, and its applications to sar images," *IEEE Transactions on Geoscience and Remote Sensing*, vol. 60, pp. 1–19, 2022.
- [22] J. Canny, "A computational approach to edge detection," *IEEE Transactions on Pattern Analysis and Machine Intelligence*, vol. PAMI-8, pp. 679–698, 1986.
- [23] C. Liu, R. Abergel, Y. Gousseau, and F. Tupin, "Ldsar, a markovian a contrario framework for line segment detection in sar images," *Pattern Recognition*, vol. 98, 2020.
- [24] C. Galamhos, J. Matas, and J. Kittler, "Progressive probabilistic hough transform for line detection," in *Proceedings. 1999 IEEE Computer Society Conference on Computer Vision and Pattern Recognition (Cat. No PR00149)*, vol. 1, 1999, pp. 554–560.
- [25] K. Yang, S. S. Ge, and H. He, "Robust line detection using twoorthogonal direction image scanning," *Computer Vision and Image Understanding*, vol. 115, pp. 1207–1222, 2011.
- [26] D. Shi, J. Gao, P. S. Rahmdel, M. Antolovich, and T. Clark, "Und: Unite-and-divide method in fourier and radon domains for line segment detection," *IEEE Transactions on Image Processing*, vol. 22, pp. 2501–2506, 2013.
- [27] R. Pautrat, D. Barath, V. Larsson, M. R. Oswald, and M. Pollefeys, "Deepplsd: Line segment detection and refinement with deep image gradients," in *2023 IEEE/CVF Conference on Computer Vision and Pattern Recognition (CVPR)*, 2023, pp. 17 327–17 336.
- [28] Q. Meng, J. Zhang, Q. Hu, X. He, and J. Yu, "Lgmn: A context-aware line segment detector," in *Proceedings of the 28th ACM International Conference on Multimedia*, 2020, pp. 4364–4372.
- [29] Y. Lin, S. L. Pintea, and J. C. van Gemert, "Deep hough-transform line priors," in *European Conference on Computer Vision*, 2020.

- [30] Y. Xu, W. Xu, D. Cheung, and Z. Tu, "Line segment detection using transformers without edges," in *2021 IEEE/CVF Conference on Computer Vision and Pattern Recognition (CVPR)*, 2021, pp. 4255–4264.
- [31] N. Carion, F. Massa, G. Synnaeve, N. Usunier, A. Kirillov, and S. Zagoruyko, "End-to-end object detection with transformers," in *European Conference on Computer Vision*, 2020, pp. 213–229.
- [32] X. Dai, H. Gong, S. Wu, X. Yuan, and Y. Ma, "Fully convolutional line parsing," *Neurocomputing*, vol. 506, pp. 1–11, 2022.
- [33] L. Teplyakov, L. Erlygin, and E. Shvets, "Lsdnet: Trainable modification of lsd algorithm for real-time line segment detection," *IEEE Access*, vol. 10, pp. 45 256–45 265, 2022.
- [34] G. Gu, B. Ko, S. Go, S.-H. Lee, J. Lee, and M. Shin, "Towards lightweight and real-time line segment detection," in *Proceedings of the AAAI Conference on Artificial Intelligence*, 2022.
- [35] M. Sandler, A. Howard, M. Zhu, A. Zhmoginov, and L.-C. Chen, "Mobilenetv2: Inverted residuals and linear bottlenecks," in *2018 IEEE/CVF Conference on Computer Vision and Pattern Recognition*, 2018, pp. 4510–4520.
- [36] C. Liu, F. Tupin, and Y. Gousseau, "Training cnns on speckled optical dataset for edge detection in sar images," *ISPRS Journal of Photogrammetry and Remote Sensing*, vol. 170, pp. 88–102, 2020.
- [37] M. Pu, Y. Huang, Y. Liu, Q. Guan, and H. Ling, "Edter: Edge detection with transformer," in *Proceedings of the IEEE/CVF Conference on Computer Vision and Pattern Recognition (CVPR)*, 2022, pp. 1402–1412.
- [38] C. Liu, C. Wang, F. Dong, X. Xiao, X. Su, C. Zhu, D. Zhang, and Q. Li, "Msmsfnet: a multi-stream and multi-scale fusion net for edge detection," *arXiv*, 2024.
- [39] J. Jie, Y. Guo, G. Wu, J. Wu, and B. Hua, "Edgenat: Transformer for efficient edge detection," *arXiv*, 2024.
- [40] A. Hassani and H. Shi, "Dilated neighborhood attention transformer," *arXiv*, 2022.
- [41] X. Soria, A. Sappa, P. Humanante, and A. Akbarinia, "Dense extreme inception network for edge detection," *Pattern Recognition*, vol. 139, p. 109461, 2023.
- [42] J. Deng, W. Dong, R. Socher, L.-J. Li, K. Li, and F.-F. Li, "Imagenet: A large-scale hierarchical image database," in *2009 IEEE Conference on Computer Vision and Pattern Recognition*, 2009, pp. 248–255.
- [43] P. Dollar and C. L. Zitnick, "Fast edge detection using structured forests," *IEEE Transactions on Pattern Analysis and Machine Intelligence*, vol. 37, pp. 1558–1570, 2015.